An optimization approach to multi-dimensional time domain acoustic inverse problems

Gustafsson, Mats; He, Sailing

1997

Total number of authors:
2

An optimization approach to multi-dimensional time domain acoustic inverse problems

Mats Gustafsson and Sailing He

Mats Gustafsson

Department of Electroscience
Electromagnetic Theory
Lund Institute of Technology
P.O. Box 118
SE-221 00 Lund
Sweden

Sailing He

Department of Electromagnetic Theory
Royal Institute of Technology
SE-100 44 Stockholm
Sweden

Abstract

An optimization approach to a multi-dimensional acoustic inverse problem in the time domain is considered. The density and/or the velocity are reconstructed by minimizing an objective functional. By introducing dual functions and using the Gauss divergence theorem, the gradient of the objective functional is found as an explicit expression. The parameters are then reconstructed by an iterative algorithm (the conjugate gradient method). The reconstruction algorithm is tested with noisy data, and these tests indicate that the algorithm is stable and robust. The computation time for the reconstruction is greatly improved when the analytic gradient is used.

1   Introduction

Acoustic inverse problems have been studied with various methods (see *e.g.*, Refs. 2, 3, 12, 13, 16, 18, 20). Recent developments and applications of various optimization methods have provided efficient tools for obtaining numerical solutions to various types of inverse problems (see *e.g.*, Refs. 1, 8, 10, 15). Optimization methods can be grouped into two types, namely, global search methods and gradient search methods. A global search method is usually based on a stochastic algorithm, and its convergence can be very slow. A gradient search method is based on a deterministic algorithm, and it converges rapidly (though it may converge to a local minimum). In order to apply a gradient search method to an inverse problem, one first introduces a suitable objective functional, and then computes the gradient of this functional. Once the gradient of the objective functional has been computed, one can use a conventional steepest descent method or conjugate gradient method to minimize the objective functional in an iterative way.

Most of the literature in this field concerning multi-dimensional inverse problems deals with frequency domain problems. For a time domain multi-dimensional inverse problem, the computation is usually more memory- and time-consuming. Therefore, it is of great importance to find a reconstruction algorithm which can complete the reconstruction within a reasonable time (say *e.g.*, a few hours on a modern workstation).

In the present paper, we use an optimization algorithm with an analytic gradient, which improves greatly the speed of the reconstruction. Wave-splitting is used to formulate a direct problem which can be solved easily by a finite difference method. Wave-splitting means the decomposition of the total field into two components which propagate in opposite directions [9]. Dual functions are introduced to derive an explicit expression for the gradient. It is shown that by using wave-splitting one obtains a simple expression for the gradient and a robust algorithm.

The paper is organized as follows. A multi-dimensional time domain acoustic inverse problem is formulated in Section 2. In Section 3, a simple explicit expression for the gradient of the objective functional is derived by introducing some dual functions and using the Gauss divergence theorem. A numerical reconstruction algorithm based on a conjugate gradient method is described in Section 4.
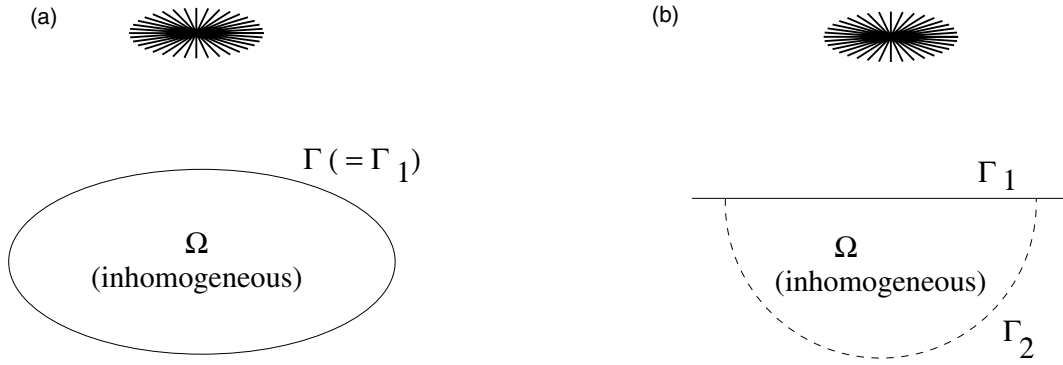
Figure 1: Scattering configurations: (a) the case of a finite object; (b) the half-space case.

2   Problem formulation

The formulation presented in this section and in Section 3 is valid in two or three spatial dimensions. The numerical implementation in Section 4, however, is only made in two spatial dimensions.

Consider wave propagation in an inhomogeneous acoustic region $\Omega \subset \mathbb{R}^3($ or $\mathbb{R}^2)$, which is described by the following stress-strain system of equations for fluids [4]

$$\begin{cases} \dfrac{1}{\rho c^2}\partial_t p + \nabla \cdot \mathbf{v} = 0, \\ \rho \partial_t \mathbf{v} + \nabla p = 0, \end{cases} \tag{2.1}$$

where p is the pressure, $\mathbf{v}$ is the velocity (the time derivative of the displacement), ρ is the fluid density, and c is the sound speed in the medium. Outside the region Ω, the medium is homogeneous with the sound speed c_0 and the density ρ_0.   It is assumed that the source has compact spatial support and is located outside the surface Γ of the inhomogeneous region Ω. It is also assumed that the incident wave will not reach the surface Γ until the time $t = 0$. This leads to the following initial conditions

$$p(x,0) = 0, \qquad \mathbf{v}(x,0) = 0, \qquad x \in \Omega. \tag{2.2}$$

In the inverse problem, it is assumed that the pressure p and the normal component of the velocity, v_n, are known for $t \in [0,T]$ on Γ_1, which is a part of the surface Γ, *i.e.*,

$$p(x,t) = p^{(m)}(x,t), \quad v_n(x,t) \equiv \mathbf{v} \cdot \hat{\mathbf{n}} = v_n^{(m)}(x,t), \quad x \in \Gamma_1, \quad t \in [0,T], \tag{2.3}$$

where $\hat{\mathbf{n}}$ is the unit normal vector of the surface Γ, $p^{(m)}(x,t)$, and $v_n^{(m)}(x,t)$ are known functions on surface Γ_1 and for the period $t \in [0,T]$. The inverse problem is to determine the density $\rho(x)$ and/or the velocity $c(x)$ in the inhomogeneous region Ω (the parameters at the surface Γ_1 are assumed to be known). Furthermore, we

assume that the incident wave have not reached the surface $\Gamma_2 = \Gamma \backslash \Gamma_1$ at the time $t = T$, *i.e.*,

$$p(x, t) = 0, \qquad \mathbf{v}(x, t) = 0, \qquad x \in \Gamma_2, \quad t \in [0, T]. \tag{2.4}$$

In the case when the inhomogeneity is confined in a bounded region Ω, one can measure p and v_n on the whole surface Γ, and thus set $\Gamma_2 = \emptyset$ (see Figure 1(a)). In another case when the inhomogeneity exists in a half-space (the medium above the inhomogeneous half-space is homogeneous with sound speed c_0 and density ρ_0), one can choose Γ_1 on the surface of the half-space large enough so that there exists a surface Γ_2 (in the inhomogeneous half-space) on which the condition (2.4) holds (see Figure 1(b)).

Introduce the following split pressures $p^{\pm}$ at the boundary Γ:

$$p^{\pm} = \frac{1}{2}[p \mp \rho_0 c_0 v_n], \qquad x \in \Gamma.$$

Note that p^+ and p^- have a physical meaning as incident (in-coming) and scattered (out-going) pressures, respectively, only in a homogeneous region (characterized by c_0 and ρ_0) and in a local sense as a normally incident or reflected plane wave. One of the main advantage of using such a splitting is that a simple expression for the gradient can be obtained in a strict sense with energy estimate methods (cf. (3.2)). Numerically it has advantages for the direct solver, as it is *e.g.*, simpler to implement the boundary condition (cf. Subsection 4.1 below). From the above definition, one has

$$\begin{cases} p = p^+ + p^-, \\ v_n = \dfrac{1}{\rho_0 c_0}[p^- - p^+] \end{cases} \quad x \in \Gamma.$$

Define an objective functional $J(\rho, c)$ as follows,

$$\begin{aligned} J(\rho, c) &\equiv \int_0^T \int_{\Gamma_1} \Phi \left\{ \left[p - p^{(m)} \right]^2 + \rho_0^2 c_0^2 \left[v_n - v_n^{(m)} \right]^2 \right\} \, \mathrm{d}S \, \mathrm{d}t \\ &= 2 \int_0^T \int_{\Gamma_1} \Phi \left\{ \left[p^+ - p^{(m)+} \right]^2 + \left[p^- - p^{(m)-} \right]^2 \right\} \, \mathrm{d}S \, \mathrm{d}t, \end{aligned} \tag{2.5}$$

where $\Phi = \Phi(x, t)$ is a weight function, $\mathrm{d}S$ is a surface area element, and

$$p^{(m)\pm} = \frac{1}{2} \left[p^{(m)} \mp \rho_0 c_0 v_n^{(m)} \right], \qquad x \in \Gamma.$$

The inverse problem is to find a function $\rho(x)$ and/or $c(x)$ which minimizes $J(\rho, c)$. The minimum of $J(\rho, c)$ is zero if the inverse problem has a solution. In the present paper we treat p^+ as the input to the optimization algorithm and p^- as the corresponding output, *i.e.*,

$$p^+ = p^{(m)+}, \qquad x \in \Gamma_1, \quad t \in [0, T]. \tag{2.6}$$

3 Explicit expression for the gradient

Let $\tilde{p}$, $\tilde{\mathbf{v}}$ be the solution to the system of equations (2.1), (2.2), (2.4), and (2.6) with perturbed parameters $\rho + \delta\rho$, $c + \delta c$. Then $\delta p \equiv \tilde{p} - p$ and $\delta\mathbf{v} \equiv \tilde{\mathbf{v}} - \mathbf{v}$ satisfy the following system of equations (obtained by taking the first order approximation):

$$
\begin{cases}
\dfrac{1}{\rho c^2}\partial_t(\delta p) + \nabla \cdot \delta\mathbf{v} = -\left(\dfrac{\delta\rho}{\rho} + \dfrac{2\delta c}{c}\right)\nabla \cdot \mathbf{v}, \\[2mm]
\rho\partial_t\delta\mathbf{v} + \nabla\delta p = \dfrac{\delta\rho}{\rho}\nabla p, \\[2mm]
\delta p(x,t) = 0, \qquad \delta\mathbf{v}(x,t) = 0, \qquad x \in \Gamma_2, \quad t \in [0,T], \\[2mm]
\delta p^+ = 0, \qquad x \in \Gamma_1, \quad t \in [0,T], \\[2mm]
\delta p(x,0) = 0, \qquad \delta\mathbf{v}(x,0) = 0, \qquad x \in \Omega.
\end{cases}
\tag{3.1}
$$

The corresponding increment of the objective functional $J(\rho, c)$ can then be written as follows:

$$
\begin{aligned}
\delta J(\rho, c) &\equiv J(\rho + \delta\rho, c + \delta c) - J(\rho, c) \\
&= 2\int_0^T\int_{\Gamma_1}\Phi\left[(p^+ + \delta p^+ - p^{(m)+})^2 + (p^- + \delta p^- - p^{(m)-})^2\right. \\
&\qquad \left. - (p^+ - p^{(m)+})^2 - (p^- - p^{(m)-})^2\right]\,\mathrm{d}S\,\mathrm{d}t \\
&= 2\int_0^T\int_{\Gamma_1}\Phi\left[\delta p^+(2p^+ - 2p^{(m)+} + \delta p^+) + \delta p^-(2p^- - 2p^{(m)-} + \delta p^-)\right]\,\mathrm{d}S\,\mathrm{d}t \\
&= 4\int_0^T\int_{\Gamma_1}\Phi\left[\delta p^+(p^+ - p^{(m)+}) + \delta p^-(p^- - p^{(m)-}) + (\delta p^+)^2 + (\delta p^-)^2\right]\,\mathrm{d}S\,\mathrm{d}t \\
&= 4\int_0^T\int_{\Gamma_1}\delta p^-\left[\Phi(p^- - p^{(m)-})\right]\,\mathrm{d}S\,\mathrm{d}t + \mathrm{O}(\|\delta\rho\|^2 + \|\delta c\|^2),
\end{aligned}
\tag{3.2}
$$

where $\mathrm{O}(x)/x$ is bounded as x approaches 0, and $\|\ \|$ denotes the L^2 norm, *i.e.*, $\|F(x)\| = \{\int_\Omega[F(x)]^2\,\mathrm{d}x\}^{1/2}$. The estimate given by the above equation can be proved with energy estimate methods (see *e.g.*, Refs. 11 and 7).

We use a direct solver for the following forward problem:

$$
\begin{cases}
\dfrac{1}{\rho c^2}\partial_t p + \nabla \cdot \mathbf{v} = 0, \\[2mm]
\rho\partial_t\mathbf{v} + \nabla p = 0, \\[2mm]
p^+ = p^{(m)+}, \qquad x \in \Gamma_1, \quad t \in [0,T], \\[2mm]
p(x,0) = 0, \mathbf{v}(x,0) = 0,
\end{cases}
\tag{3.3}
$$

and the following backward dual problem:

$$\begin{cases} \dfrac{1}{\rho c^2}\partial_t q + \nabla \cdot \mathbf{u} = 0, \\[2mm] \rho\partial_t \mathbf{u} + \nabla q = 0, \\[2mm] q^- = \Phi[p^- - p^{(m)-}], \qquad x \in \Gamma_1, \quad t \in [0, T], \\[2mm] q(x, T) = 0, \qquad \mathbf{u}(x, T) = 0, \end{cases} \tag{3.4}$$

where

$$q^{\pm} = \frac{1}{2}[q \mp \rho_0 c_0 u_n], \qquad x \in \Gamma.$$

Note that (cf. (2.4))

$$q(x, t) = 0, \qquad \mathbf{u}(x, t) = 0, \qquad x \in \Gamma_2, \quad t \in [0, T].$$

The system (3.3) is solved by a finite difference method with a forward time stepping, and the system (3.4) is solved by a finite difference method with a backward time stepping. In order to avoid any inconsistency between the boundary and initial conditions in the system (3.4), one should choose the weight function such that

$$\Phi(x, T) = 0.$$

Using the differential equations in the systems (3.1), (3.3) and (3.4), one obtains

$$\nabla \cdot (\delta p \mathbf{u} + q \delta \mathbf{v}) = [\nabla(\delta p)] \cdot \mathbf{u} + \delta p \nabla \cdot \mathbf{u} + (\nabla q) \cdot \delta \mathbf{v} + q \nabla \cdot (\delta \mathbf{v})$$

$$= -\partial_t \left[\frac{1}{\rho c^2}(\delta p)q + \rho(\delta \mathbf{v}) \cdot \mathbf{u} \right] + \frac{\delta \rho}{\rho}[-q\nabla \cdot \mathbf{v} + (\nabla p) \cdot \mathbf{u}] - \frac{2\delta c}{c}q\nabla \cdot \mathbf{v}$$

$$= -\partial_t \left[\frac{1}{\rho c^2}(\delta p)q + \rho(\delta \mathbf{v}) \cdot \mathbf{u} \right] + \frac{\delta \rho}{\rho}[-q\nabla \cdot \mathbf{v} + \nabla \cdot (p\mathbf{u}) - p\nabla \cdot \mathbf{u}] - \frac{2\delta c}{c}q\nabla \cdot \mathbf{v}$$

$$= -\partial_t \left[\frac{1}{\rho c^2}(\delta p)q + \rho(\delta \mathbf{v}) \cdot \mathbf{u} - \frac{\delta \rho}{\rho^2 c^2}(qp) \right] + \frac{\delta \rho}{\rho}\nabla \cdot (p\mathbf{u}) - \frac{2\delta c}{c}q\nabla \cdot \mathbf{v}.$$

Integrating the above equation over the time period $[0, T]$ and the region Ω and using the Gauss divergence theorem, one obtains

$$\int_0^T \int_\Gamma (\delta p \mathbf{u} + q \delta \mathbf{v}) \cdot \hat{\mathbf{n}}\, \mathrm{d}S\, \mathrm{d}t = \int_0^T \int_\Omega \frac{\delta \rho}{\rho}\nabla \cdot (p\mathbf{u})\, \mathrm{d}x\, \mathrm{d}t - 2\int_0^T \int_\Omega \frac{\delta c}{c}q\nabla \cdot \mathbf{v}\, \mathrm{d}x\, \mathrm{d}t. \tag{3.5}$$

Since (cf. (3.2) and noting that $\delta p^+ = 0$ and $q^- = \Phi(p^- - p^{(m)-})$)

$$
\int_0^T \int_\Gamma (\delta p \mathbf{u} + q \delta \mathbf{v}) \cdot \hat{\mathbf{n}} \, \mathrm{d}S \, \mathrm{d}t = \int_0^T \int_{\Gamma_1} (\delta p u_n + q \delta v_n) \, \mathrm{d}S \, \mathrm{d}t
$$

$$
= -\frac{1}{\rho_0 c_0} \int_0^T \int_{\Gamma_1} \left[(\delta p^+ + \delta p^-)(q^+ - q^-) + (\delta p^+ - \delta p^-)(q^+ + q^-) \right] \, \mathrm{d}S \, \mathrm{d}t
$$

$$
= -\frac{2}{\rho_0 c_0} \int_0^T \int_{\Gamma_1} \left[\delta p^+ q^+ - \delta p^- q^- \right] \, \mathrm{d}S \, \mathrm{d}t = \frac{2}{\rho_0 c_0} \int_0^T \int_{\Gamma_1} (\delta p^-) q^- \, \mathrm{d}S \, \mathrm{d}t
$$

$$
= \frac{2}{\rho_0 c_0} \int_0^T \int_{\Gamma_1} (\delta p^-) \Phi \left[p^- - p^{(m)-} \right] \, \mathrm{d}S \, \mathrm{d}t = \frac{1}{2\rho_0 c_0} \delta J(\rho, c) + \mathrm{O}(\|\delta \rho\|^2 + \|\delta c\|^2),
$$

it follows from (3.5) that

$$
\delta J = < G_\rho, \delta \rho > + < G_c, \delta c > + \mathrm{O}(\|\delta \rho\|^2 + \|\delta c\|^2),
$$

where $< , >$ denotes the inner product (with respect to the spatial region Ω) and

$$
\begin{cases}
G_\rho = \dfrac{2\rho_0 c_0}{\rho} \displaystyle\int_0^T \nabla \cdot (\mathbf{u} p) \, \mathrm{d}t, & x \in \Omega, \\[3mm]
G_c = -\dfrac{4\rho_0 c_0}{c} \displaystyle\int_0^T q \nabla \cdot \mathbf{v} \, \mathrm{d}t = \dfrac{4\rho_0 c_0}{\rho c^3} \displaystyle\int_0^T q \partial_t p \, \mathrm{d}t, & x \in \Omega
\end{cases}
\tag{3.6}
$$

Equation (3.6) gives the explicit expressions for the gradients of the objective functional $J(\rho, c)$ with respect to the density $\rho(x)$ and the sound speed $c(x)$, respectively.

Note that the results given in this subsection are valid for arbitrary number n of space dimensions, $n \geq 2$.

4   Parameter reconstruction

In this section we use an optimization algorithm (the conjugate gradient algorithm) with the analytic gradients derived in the previous section to reconstruct the density and sound speed in the two-dimensional case (i.e., $x = (x_1, x_2)$ in all the formulas given in the previous sections).

4.1   The direct solver

We use both a leapfrog scheme and a Lax-Wendroff scheme to solve the systems (3.3) and (3.4) (cf. e.g., Refs. 17 and 6).

A leapfrog scheme. Let $p_{i,j}^n$ denote an approximation of p at $t = nk$, $x_1 = ih$ and $x_2 = jh$, and similarly for $\mathbf{v}_{i,j}^n$. At interior points the leapfrog scheme becomes

$$
\begin{cases}
p_{i,j}^{n+1} = p_{i,j}^{n-1} - \rho_{i,j} c_{i,j}^2 2k \nabla_0 \cdot \mathbf{v}_{i,j}^n \\[3mm]
\mathbf{v}_{i,j}^{n+1} = \mathbf{v}_{i,j}^{n-1} - \dfrac{2}{\rho_{i,j}} k \nabla_0 p_{i,j}^n
\end{cases}
$$

where ∇_0 is the central difference nabla operator (*i.e.*, $\nabla_0 f_{i,j} = (f_{i+1,j} - f_{i-1,j}, f_{i,j+1} - f_{i,j-1})/2h$). For a finite inhomogeneous object located in a square area $(x_1, x_2) \in [0,1] \times [0,1]$, the fields at the boundary are computed with a one way propagation type of scheme. For example, at the left boundary $x_1 = 0$, the differential equations in (2.1) are equivalent to the following system of differential equations (for simplicity, here we assume that $\rho_0 = c_0 = 1$)

$$\begin{cases} \partial_t p^\pm \pm \partial_{x_1} p^\pm + \dfrac{1}{2} \nabla_\mathrm{T} \cdot \mathbf{v}_\mathrm{T} = 0, \\ \partial_t \mathbf{v}_\mathrm{T} + \nabla_\mathrm{T} p = 0, \end{cases}$$

where we have used the split fields $p^\pm = \frac{1}{2}[p \mp \rho_0 c_0 v_n] = (p \pm v_1)/2$ at the left boundary $x_1 = 0$, and the subscript T is used to denote the tangential component. The above system of equations can be implemented numerically as follows:

$$\begin{cases} (p^+)_{0,j}^{n+1} = (p^{(m)+})_{0,j}^{n+1}, \quad \text{(cf. the boundary condition (2.6))} \\ (p^-)_{0,j}^{n+1} = (p^-)_{0,j}^n + \dfrac{k}{h}\left[(p^-)_{1,j}^n - (p^-)_{0,j}^n\right] - \dfrac{k}{2}(\nabla_\mathrm{T})_0 \cdot (\mathbf{v}_\mathrm{T})_{0,j}^n, \\ p_{0,j}^{n+1} = (p^+)_{0,j}^{n+1} + (p^-)_{0,j}^{n+1}, \\ (v_1)_{0,j}^{n+1} = (p^+)_{0,j}^{n+1} - (p^-)_{0,j}^{n+1}, \\ (\mathbf{v}_\mathrm{T})_{0,j}^{n+1} = (\mathbf{v}_\mathrm{T})_{0,j}^{n-1} - 2k(\nabla_\mathrm{T})_0 p_{0,j}^n. \end{cases}$$

The boundary conditions at the other boundaries are treated similarly.

A Lax-Wendroff scheme. The Lax-Wendroff scheme is based on the following Taylor series approximation,

$$\begin{cases} p^{n+1} = p^n - k\rho c^2 \nabla \cdot \mathbf{v}^n + \dfrac{k^2}{2}\rho c^2 \nabla \cdot \left(\dfrac{1}{\rho}\nabla p^n\right), \\ \mathbf{v}^{n+1} = \mathbf{v}^n - \dfrac{k}{\rho}\nabla p^n + \dfrac{k^2}{2\rho}\nabla\left(\rho c^2 \nabla \cdot \mathbf{v}^n\right), \end{cases}$$

with the second order approximations for the spatial derivatives. The fields at the boundary are treated in a way that is similar to the one used in the leapfrog scheme, except that the tangential components are implemented with a Lax-type scheme, *e.g.*, ,

$$(\mathbf{v}_\mathrm{T})_{0,j}^{n+1} = \frac{1}{2}(\mathbf{v}_\mathrm{T})_{0,j-1}^n + \frac{1}{2}(\mathbf{v}_\mathrm{T})_{0,j+1}^n - k(\nabla_\mathrm{T})_0 p_{0,j}^n,$$

at the left boundary $x_1 = 0$.

In the gradient calculation the leapfrog scheme is used to simulate the systems (3.3) and (3.4), as well as in the calculation of the objective functional defined by (2.5). The Lax-Wendroff scheme is used to calculate the measured fields $p^{(m)}(x,t)$ and $v_n^{(m)}$ at the boundary (cf. (2.3)). Since the measured data are calculated in a way that is different from what is used for the direct solver, we avoid the 'inverse crime' when solving the inverse problem [3].

4.2 The conjugate gradient method

Once the gradient of the objective functional has been computed, one can use a conventional steepest descent method or conjugate gradient method to minimize the objective functional in an iterative way. The steepest descent method usually exhibits slower convergence rates than the conjugate gradient method [5]. In the present paper we use a standard conjugate gradient method (Polak-Ribiere algorithm [5, 14]) to minimize the objective functional and reconstruct the density $\rho(x_1, x_2)$ or the sound speed $c(x_1, x_2)$. The iterative algorithm for the reconstruction of $\rho(x_1, x_2)$ is as follows:

Step 0: Select an initial approximation (guess) $\rho = \rho^{(0)}(x_1, x_2)$. In all our numerical reconstructions, we take the initial approximation $\rho = \rho_0$ (the constant density value outside the region Ω).

Step 1: Set $i = 0$. Solve the direct problem for the system (3.3) with the leapfrog scheme, and calculate the gradient $G^{(0)} = G(\rho^{(0)})$ using (3.6) ($\mathbf{u}$ is obtained by solving the system (3.4) with the leapfrog scheme). Set $H^{(0)} = G^{(0)}$.

Step 2: Compute a scalar stepsize $\lambda_i > 0$ in the line search such that

$$J(\rho^{(i)} - \lambda_i H^{(i)}) = \min\{J(\rho^{(i)} - \lambda H^{(i)}) | \lambda \geq 0\}.$$

Step 3: Improve the reconstruction by setting

$$\rho^{(i+1)} = \rho^{(i)} - \lambda_i H^{(i)}.$$

Step 4: Compute the new gradient $G^{(i+1)} = G(\rho^{(i+1)})$ using (3.6) (p and $\mathbf{u}$ are obtained by solving the systems (3.3) and (3.4), respectively, with the leapfrog scheme).

Step 5: If $G^{(i+1)} = 0$, stop; if not, set

$$H^{(i+1)} = G^{(i+1)} + \gamma_i H^{(i)}, \quad \text{with } \gamma_i = \frac{< G^{(i+1)} - G^{(i)}, G^{(i+1)} >}{< G^{(i)}, G^{(i)} >},$$

and set $i = i + 1$, and go to step 2.

4.3 Regularization

The parameter reconstruction is ill-posed in the sense that the high frequency part of the parameter is not known. To get a smooth solution we regularize the problem with a Tikhonov type of regularization.

For example, in the reconstruction of the density $\rho(x_1, x_2)$, we add a term $\int_\Omega \alpha |\nabla \rho|^2 \, \mathrm{d}x$ to the objective functional, i.e.,

$$J_\alpha(\rho) = J(\rho) + \int_\Omega \alpha(x)|\nabla \rho|^2 \, \mathrm{d}x.$$

The corresponding increment in the objective functional is

$$\int_\Omega \alpha\{|\nabla(\rho+\delta\rho)|^2 - |\nabla\rho|^2\}\,\mathrm{d}x = \int_\Omega \alpha\{\nabla\delta\rho \cdot \nabla(2\rho+\delta\rho)\}\,\mathrm{d}x$$

$$= 2\int_\Omega \{\nabla \cdot [\delta\rho\alpha\nabla\rho] - \delta\rho\nabla \cdot [\alpha\nabla\rho]\}\,\mathrm{d}x + \int_\Omega \alpha|\nabla\delta\rho|^2\,\mathrm{d}x$$

$$= 2\int_\Gamma \alpha\delta\rho\partial_n\rho\,\mathrm{d}S - 2\int_\Omega \{\delta\rho\nabla \cdot [\alpha\nabla\rho]\}\,\mathrm{d}x + \int_\Omega \alpha|\nabla\delta\rho|^2\,\mathrm{d}x.$$

Thus one obtains the following gradient with respect to the density (note that $\delta\rho|_\Gamma = 0$),

$$G_{\rho,\alpha} = \frac{2}{\rho}\int_0^T \nabla \cdot (\mathbf{u}p)\,\mathrm{d}t - 2\nabla \cdot [\alpha\nabla\rho].$$

The optimal value of the regularization parameter α can be determined by the generalized cross validation method [19].

We can also force ρ at the boundary to assume the known values ρ_b, by adding a term $\beta\int_\Omega \Psi|\rho - \rho_b|^2\,\mathrm{d}x$ to the objective functional, *i.e.*,

$$J_\beta(\rho) = J(\rho) + \beta\int_\Omega \Psi|\rho - \rho_b|^2\,\mathrm{d}x,$$

where ρ_b is the known value of ρ at the boundary. The weight function $\Psi(x)$ is large when x is close to the boundary and small in the interior region. In all the numerical reconstructions given in next subsection we use $\Psi(x) = \mathrm{e}^{-0.5[\gamma(x)]^2}$, where $\gamma(x)$ is the distance to the boundary. The corresponding increment in the objective functional is

$$\int_\Omega \Psi\{|\rho + \delta\rho - \rho_b|^2 - |\rho - \rho_b|^2\}\,\mathrm{d}x = \int_\Omega \Psi\delta\rho(2(\rho - \rho_b) + \delta\rho)\,\mathrm{d}x$$

$$= 2\int_\Omega \Psi\delta\rho(\rho - \rho_b)\,\mathrm{d}x + \int_\Omega \Psi\delta\rho^2\,\mathrm{d}x.$$

Thus, one obtains the following gradient with respect to the density (note that $\delta\rho|_\Gamma = 0$),

$$G_{\rho,\beta} = \frac{2}{\rho}\int_0^T \nabla \cdot (\mathbf{u}p)\,\mathrm{d}t - 2\beta\Psi(\rho - \rho_b).$$

4.4   Reconstruction results

In a first numerical example, we consider an inhomogeneous density profile in a square area $(x_1, x_2) \in [0,1] \times [0,1]$ as shown in Figure 2(a). The sound speed is a constant $c = c_0 = 1$. The inhomogeneous square region is discretized by 72×72 equidistant grid points. One Gaussian pulse of p^+ is used as a source illuminating the square from the left side (as shown in Figure 3(a)), and the scattered fields are measured on all the four sides of the square (as shown in Figure 3(b)). In the
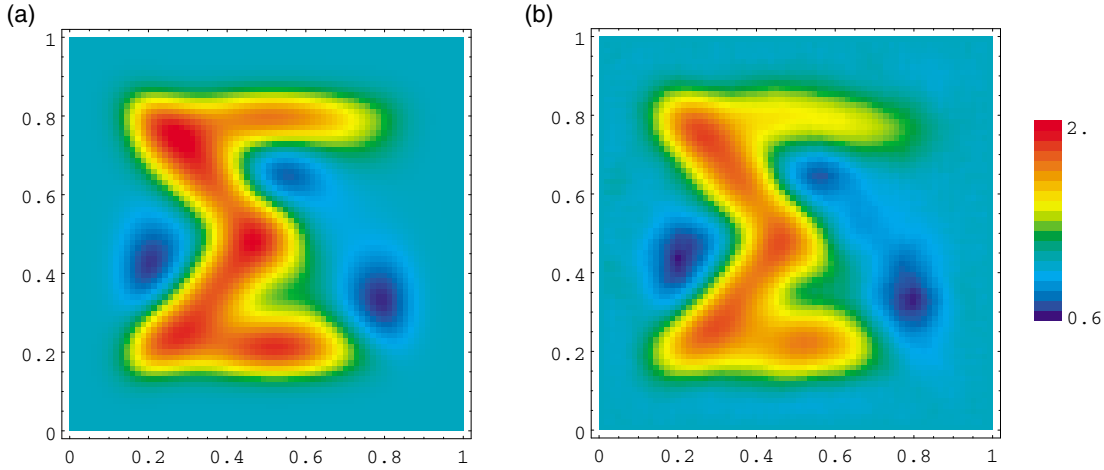
Figure 2: Reconstruction of the density profile in a square area using one Gaussian pulse at the left side of the square. (a) the true density profile; (b) the reconstruction.

time-space plots of Figures 3(a) and 3(b), the four $t = 0$ lines correspond, from left to right, respectively, to the up, left, down, and right sides. The 'measured' data are simulated with the Lax-Wendroff scheme. The fields are measured in a time interval $[0, 2.5]$ discretized with 360 grid points. Random white noise with a root mean square signal to noise ratio (SNR_{rms}) of 11 has been added to the measured fields $p^{(m)}$ and $v_n^{(m)}$ (equivalent to $p^{(m)\pm}$). The signal to noise ratio is estimated by the following formula

$$SNR_{rms} = \frac{1}{\sigma} \left(\frac{1}{TA} \int_0^T \int_\Gamma \left(p^\pm - \bar{p}^\pm \right)^2 \, \mathrm{d}S \, \mathrm{d}t \right)^{1/2},$$

where A is the area of the boundary Γ and

$$\sigma = \left(\frac{1}{TA} \int_0^T \int_\Gamma \varepsilon^2 \, \mathrm{d}S \, \mathrm{d}t \right)^{1/2},$$

$$\bar{p}^\pm = \frac{1}{TA} \int_0^T \int_\Gamma p^\pm \, \mathrm{d}S \, \mathrm{d}t,$$

and where ε is the noise added to the fields. In the numerical reconstructions we choose the regularization parameters $\alpha = 0.001$, $\beta = 10$, and a weight function Φ that goes to zero smoothly over the last 15 time steps. The reconstructed density after 47 iterations is shown in Figure 2(b) (the starting guess is $\rho = \rho_0 = 1$ everywhere). The maximum absolute error in the density reconstruction is about 0.29. The reconstruction took about 20 minutes on a Sun workstation (Ultra 1). The reconstruction requires a memory of about 30 MByte in RAM.

The reconstruction can be improved further if 4 Gaussian pulses at four different sides of the square are used, and the corresponding reconstruction using noisy data with $SNR_{rms} = 11$ is given in Figure 4(a) (the starting guess is $\rho = \rho_0 = 1$
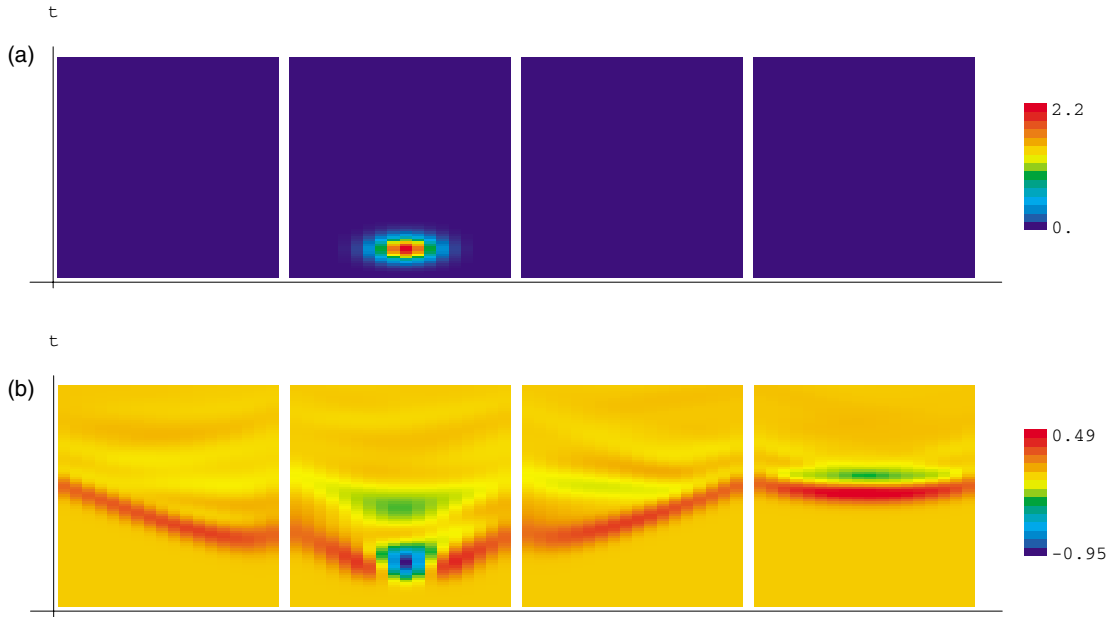
Figure 3: The measured fields at the boundary. (a) the input $p^{(m)+}$ on the four sides of the square; (b) the output $p^{(m)-}$ on the four sides of the square.

everywhere; 23 iterations are used). In this reconstruction and the reconstructions hereafter, the measured noisy data are smoothed by a weighted five point mean value smoother. For example, the data at the top and bottom sides of the square area are smoothed by

$$p_i^n = \frac{4p_i^n + p_{i-1}^n + p_{i+1}^n + p_i^{n-1} + p_i^{n+1}}{8}.$$

The reconstruction error of the density at each point of the square is shown in Figure 4(b) (note that the colour rules in Figures 4(a) and 4(b) are different). As seen from Figure 4(b), the maximum absolute error in the density reconstruction is about 0.05.

The reconstruction of the the sound speed can be performed in a completely analogous way, and an example is shown in Figures 5(a) (the true profile of the sound speed) and 5(b) (the corresponding reconstruction). In this reconstruction, noisy data with $SNR_{rms} = 11$ are used, the starting guess is $c = c_0 = 1$ everywhere, and the density is a constant $\rho = \rho_0 = 1$.

In a last numerical example, we reconstruct the density in an inhomogeneous half-space using the 'measured' fields on a *finite* area of the surface $x_2 = 0$ for a finite period of time. In this example, a wide input field p^+ (with a unit width) excites the surface $x_1 = 0$, see Figure 6. As one would expect, good reconstruction can be achieved only in a finite region (below the surface $x_1 = 0$) of the inhomogeneous half-space. The true density and the reconstructed density are shown in Figures 6(a) and 6(b), respectively. This reconstruction took about 5.5 hours on a Silicon Graphics workstation (Power Indigo2) and the memory requirement was about 150 MByte in RAM.
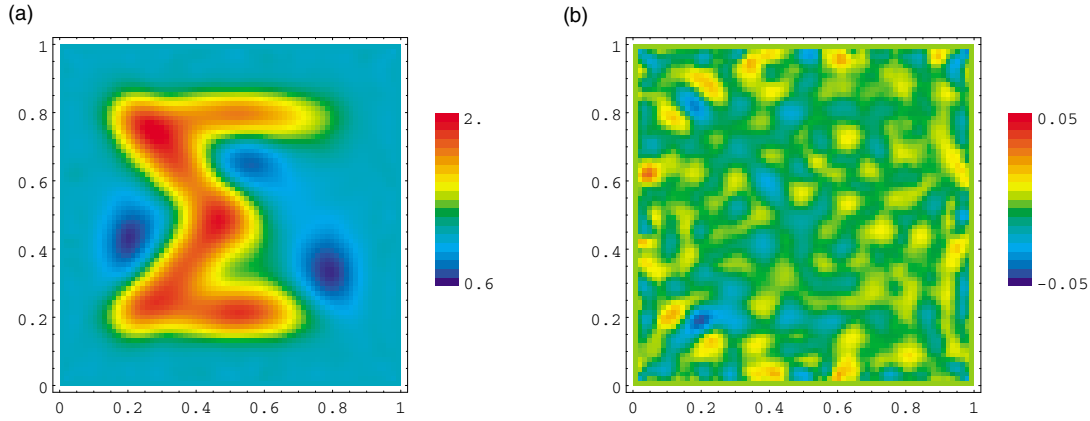
Figure 4: Reconstruction of the density profile in a square area using four Gaussian pulses at four different sides of the square (for the same density profile as shown in Figure 2(a)). (a) the reconstruction; (b) reconstruction error of the density.

4.5 Computation efficiency

We compare the computation times for the reconstructions obtained with and without the analytic gradients. When an analytic gradient is not available, one can calculate the gradient numerically through the following set of characteristic functions

$$\psi_i(x) = \begin{cases} 1, & x \in V_i, \\ 0, & \text{otherwise,} \end{cases}$$

where V_i, $i = 1, 2, ..., N$, are the discretized volume cells. Assume that $\rho(x) = \sum_i P_i \psi_i(x)$ ($\rho(x)$ is the density to be reconstructed), and the corresponding gradient $G_\rho(x) = \sum_i g_i \psi_i(x)$, then one can calculate the coefficient G_i numerically through the following approximation:

$$G_i \approx \frac{J(< P_0, P_1, ..., P_i + \varepsilon, ..., P_N >) - J(< P_0, P_1, ..., P_i, ..., P_N >)}{\varepsilon},$$

where ε is a small quantity. In the present reconstruction algorithm, the computation time is consumed mainly by calling the forward direct solver for the system (3.3) and the backward direct solver for the system (3.4) (which takes a time that is roughly equal to that for the forward direct solver). To calculate the gradient, one has to call the forward direct solver N times when the numerical perturbation is used, while using the present analytic expression, one only needs to call the forward and backward direct solvers once. Therefore, the ratio of the computation times for the gradient with and without the analytic expression is about $2/N$. In fact, the ratio of the overall computation time for the reconstruction (if the same number of iterations is required) with and without the analytic gradients is approximately $\frac{2+s}{N+1+s}$, where s is the average number of steps in the line search within each
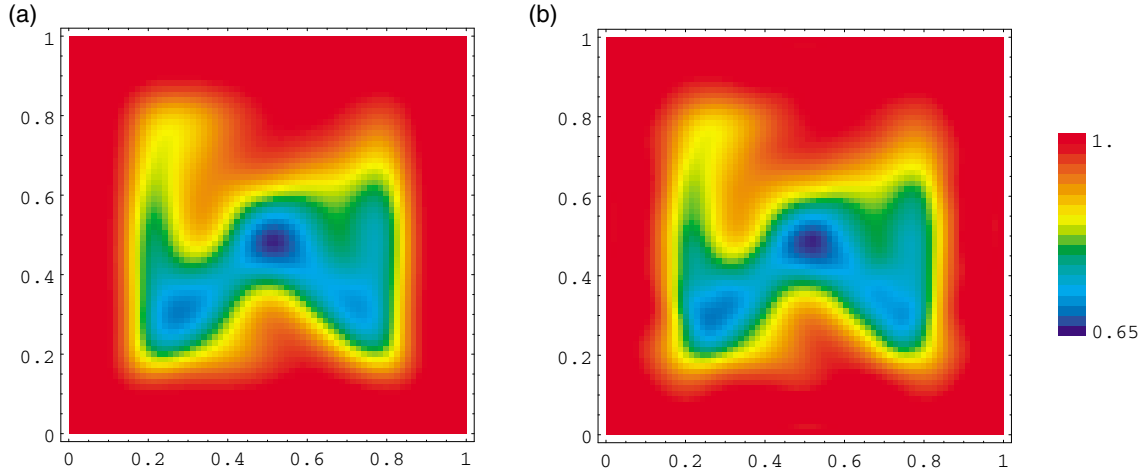
Figure 5: Reconstruction of the sound speed profile in a square area using four Gaussian pulses at the four different sides of the square. (a) the true density profile; (b) the reconstruction.

iteration ($s \approx 2$ if an optimal line search program is used). In a multi-dimensional case, N is large (if one takes N_x discretization points along each orthogonal space direction, then $N = (N_x)^n$, where $n = 2, 3$ in two- and three-dimensional cases, respectively). Therefore, the computation time required for the reconstruction can be greatly improved in a multi-dimensional case if an analytic gradient is used.

5   Conclusion

In the present paper we have treated an multi-dimensional acoustic inverse problem in the time domain with a deterministic gradient search algorithm. The density and/or the velocity are reconstructed by minimizing an objective functional with an analytic gradient. By introducing some dual functions and using the Gauss divergence theorem, explicit expression for the gradient of the objective functional has been derived. The parameters have been reconstructed by a conjugate gradient method. The reconstruction algorithm has been tested in the two-dimensional case with noisy data, and the numerical examples indicate that the algorithm is stable and robust. The computation time required for the reconstruction is significantly reduced in the multi-dimensional case when the analytic gradient is used.

Acknowledgment
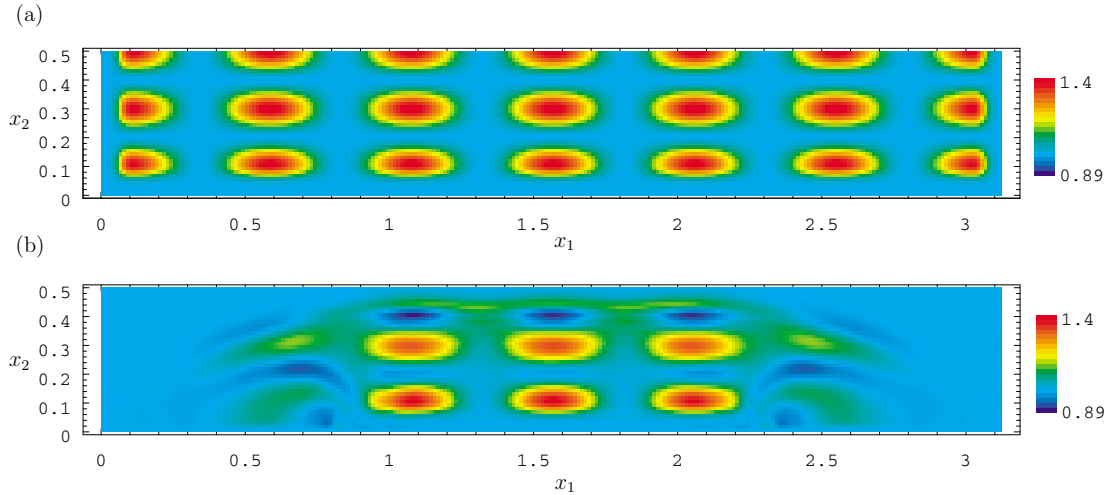
Figure 6: Reconstruction of the density profile in an inhomogeneous half-space. (a) the true density profile; (b) the reconstruction.

References

[1] A. Bamberger and G. Chavent. Inversion of normal incidence seismograms. *Geophysics*, **47**, 757–770, 1982.

[2] J. Cao and S. He. Reconstruction of the velocity and density in a stratified acoustic half-space using a short-pulse point source. *J. Acoust. Soc. Am.*, **102**(2), 815–824, 1997.

[3] D. Colton and K. R. *Inverse Acoustic and Electromagnetic Scattering Theory.* Springer-Verlag, Berlin, 1992.

[4] F. G. Friedlander. *Sound Pulses.* Cambridge University Press, Cambridge, U.K., 1958.

[5] P. E. Gill, W. Murray, and M. H. Wright. *Practical Optimization.* Academic Press, London, 1981.

[6] B. Gustafsson, H.-O. Kreiss, and J. Oliger. *Time Dependent Problems and Difference Methods.* John Wiley & Sons, New York, 1995.

[7] M. Gustafsson. Time domain theory of the macroscopic maxwell equations. Technical Report LUTEDX/(TEAT-7062)/1–24/(1997), Lund Institute of Technology, Department of Electromagnetic Theory, P.O. Box 118, S-211 00 Lund, Sweden, 1997.

[8] S. He and S. I. Kabanikhin. An optimization approach to a three-dimensional acoustic inverse problem in the time domain. *J. Math. Phys.*, **36**(8), 4028–4043, 1995.

[9] S. He, S. Ström, and V. H. Weston. *Time Domain Wave-splittings and Inverse Problems.* Oxford University Press, Oxford, 1998. In press.

[10] R. E. Kleinman and P. M. van den Berg. Non-linearized approach to profile inversion. *Int. J. Imaging Systems Tech.*, **2**, 119–126, 1990.

[11] H.-O. Kreiss and J. Lorenz. *Initial-Boundary Value Problems and the Navier-Stokes Equations.* Academic Press, San Diego, 1989.

[12] M. Moghaddam and W. C. Chew. Simultaneous inversion of compressibility and density in the acoustic inverse problem. *Inverse Problems*, **9**, 715–730, 1993.

[13] S. S. Pan, R. A. Phinney, and R. I. Odem. Full-waveform inversion of planewave seismograms in stratified acoustic media: Theory and feasibility. *Geophysics*, **53**(1), 21–31, 1988.

[14] E. Polack. *Computational Methods in Optimization, a Unified Approach.* Academic Press, New York, 1971.

[15] V. G. Romanov and S. I. Kabanikhin. *Inverse Problems of Geoelectrics.* VNU Science Press BV, Utrecht, 1994.

[16] F. Santosa, Y. Pao, W. Symes, and C. Holland, editors. *Inverse Problems of Acoustic and Elastic Waves*, SIAM Philadelphia, PA, 1984. Proc. SPIE 413.

[17] J. C. Strikwerda. *Finite Difference Schemes and Partial Differential Equations.* Chapman & Hall, New York, 1989.

[18] W. W. Symes. Impedance profile inversion via the first transport equation. *J. Math. Anal. Appl.*, **94**, 435–453, 1983.

[19] G. Wahba. Practical approximate solutions to linear operator equations when the data are noisy. *SIAM Journal on Numerical Analysis*, **14**, 651–667, 1977.

[20] A. E. Yagle and B. Levy. A fast algorithm solution of the inverse problem for a layered acoustic medium probed by spherical waves. *J. Acoust. Soc. Am.*, **78**, 729–737, 1985.